

GaussianOcc: Fully Self-supervised and Efficient 3D Occupancy Estimation with Gaussian Splatting

Wanshui Gan ^{1,2,*}Fang Liu ^{1,*}Hongbin Xu ³Ningkai Mo ⁴Naoto Yokoya ^{1,2,†}¹The University of Tokyo, ²RIKEN, ³South China University of Technology⁴Shenzhen Institute of Advanced Technology, Chinese Academy of Sciences

* Equal contribution, † Corresponding author

{wanshuigan, fangliu2896, hongbinxu1013, nk.mo19941001}@gmail.com

yokoya@k.u-tokyo.ac.jp

Abstract

We introduce GaussianOcc, a systematic method that investigates two usages of Gaussian splatting for fully self-supervised and efficient 3D occupancy estimation in surround views. First, traditional methods for self-supervised 3D occupancy estimation still require ground truth 6D poses from sensors during training. To address this limitation, we propose Gaussian Splatting for Projection (GSP) module to provide accurate scale information for fully self-supervised training from adjacent view projection. Additionally, existing methods rely on volume rendering for final 3D voxel representation learning using 2D signals (depth maps and semantic maps), which is time-consuming and less effective. We propose Gaussian Splatting from Voxel space (GSV) to leverage the fast rendering properties of Gaussian splatting. As a result, the proposed GaussianOcc method enables fully self-supervised (no ground-truth pose) 3D occupancy estimation in competitive performance with low computational cost (2.7 times faster in training and 5 times faster in rendering). The relevant code is available in <https://github.com/GANWANSHUI/GaussianOcc.git>.

1. Introduction

In recent years, both vision-centric and grid-centric perception approaches have gained significant attention in the autonomous driving industry and academia [34, 39]. Among these, surround view 3D occupancy estimation [31, 45, 48, 51] has emerged as a core perception task and a promising alternative to bird’s-eye view (BEV) methods [9, 28, 29]. To facilitate 3D occupancy estimation, several benchmarks have been developed for supervised training [41–43, 45], though these require substantial effort in

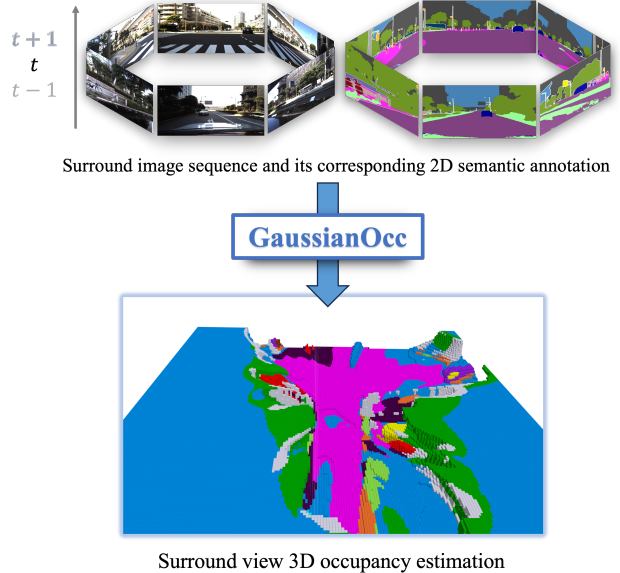


Figure 1. Problem setting of GaussianOcc. Given a surround image sequence and its corresponding 2D semantic annotation, GaussianOcc is able to perform 3D occupancy estimation without the need for ground truth occupancy label and ground truth 6D pose for training.

3D annotation. To reduce the burden of annotation, self-supervised [5, 11, 17, 23, 54] and weakly-supervised [37] learning approaches based on volume rendering have been proposed [10, 35, 46]. Volume rendering allows 3D representation learning using 2D supervision signals, such as 2D semantic maps and depth maps, thereby eliminating the need for extensive 3D annotation during training.

Existing methods [23, 54] achieve self-supervised learning through volume rendering, where the 2D semantic map supervision is derived from open-vocabulary semantic segmentation [55], and the depth map supervision is obtained from self-supervised depth estimation [12]. However, these approaches face two significant limitations. First, volume rendering is performed at real-world scale, which requires the availability of ground truth 6D pose to calculate the multi-view photometric loss across sequential images. Second, the inefficiency in volume rendering poses a challenge, the same as in novel view synthesis tasks [1, 18, 26], due to the dense sampling operation required. These limitations impede the development of a more general and efficient paradigm for self-supervised 3D occupancy estimation.

To address the aforementioned limitations, we propose a fully self-supervised and efficient approach to 3D occupancy estimation using Gaussian splatting [1, 26]. Specifically, we introduce the use of Gaussian splatting to perform cross-view splatting, where the rendered image constructs a cross-view loss that provides scale information during joint training with the 6D pose network. This eliminates the need for ground truth 6D pose during training. To improve rendering efficiency, we move away from the dense sampling required in traditional volume rendering. Instead, we propose performing Gaussian splatting directly from the 3D voxel space. In this approach, each vertex in the voxel grid is treated as a 3D Gaussian, and we optimize the attributes of these Gaussians—such as semantic features and opacity—directly within the voxel space. Through this novel approach, our proposed method, GaussianOcc, makes a progress toward fully self-supervised and efficient 3D occupancy estimation, as outlined in Figure 1.

In summary, our core contributions are as follows:

- We introduce the first fully self-supervised method for efficient surrounding-view 3D occupancy estimation, featuring the exploration of Gaussian splatting.
- We propose Gaussian splatting for cross-view projection module, which can provide scale information to get rid of the need of ground truth 6D pose during the training.
- We propose Gaussian splatting from voxel space module, achieving competitive performance with 2.7 times faster training and 5 times faster rendering compared to the previous works with volume rendering.

2. Related work

2.1. Surround view depth estimation

The surround view setting offers an ego-centric 360-degree perception solution [3, 13, 34, 39]. [16] introduces the surround view benchmark in the supervised setting, which learns the depth scale directly from the ground truth depth map. FSM [15] is a pioneering work in scale-aware surround view depth estimation relying on stereo constraint

[53]. However, subsequent studies [27, 44] have found that reproducing the performance of [15] is challenging. Surrounddepth [44] improves the scale supervision signal using sparse point clouds from Structure-from-Motion (SfM). Building on the spatial and temporal constraints in FSM, [27] introduces a volume feature fusion module to enhance performance. For better performance, [38] proposes the temporal offline refinement strategy based on the multiple cameras and monocular depth refinement. These works [15, 27, 38, 44] all use traditional projection and index interpolation for cross-view synthesis, computing the loss between the synthesized view and target images. Compared to the traditional projection, our approach employs Gaussian splatting with a dedicated design for cross-view constraint, achieving better performance.

2.2. Surround view 3D occupancy estimation

Surround view 3D occupancy estimation has gained significant attention in recent years, with several benchmarks based on the nuScenes dataset [41, 43, 45]. In addition to the advanced architectures being proposed [30, 31, 51, 56], another research trend involves utilizing volume rendering for 3D occupancy learning with 2D supervision [11, 23, 37, 54]. SimpleOcc [11] pioneered the use of volume rendering for 3D occupancy estimation, exploring both supervised and self-supervised learning. RenderOcc [37] extends semantic information for rendering. OccNeRF [54] and SelfOcc [23] share a similar approach by using 2D open-vocabulary semantic models to generate semantic maps for supervision. However, since volume rendering processes are conducted at real-world scale, these self-supervised methods [11, 23, 54] require ground truth 6D poses from sensors to provide the real-world scale for training. Differently, we are exploring a solution that utilizes the overlap region in adjacent cameras to learn the real-world scale, eliminating the need for ground truth 6D poses.

2.3. 3D Gaussian splatting

3D Gaussian splatting has become a popular method for modeling 3D and 4D scenes using well-posed images [8, 25, 26, 47], which has the property of fast rendering compared to the volume rendering in neural radiance field [10, 18, 35]. In driving scenes, a line of research has focused on scene-specific reconstruction [21, 49, 58]. Our work, however, investigates the function of Gaussian splatting in a generalized setting, where existing methods generally construct 3D Gaussians from the unprojection of learned 2D Gaussian attributes [7, 32, 40, 57]. We also employ this unprojection approach, but uniquely, our approach constructs cross-view information from adjacent views to learn scale information through Gaussian splatting projection. In addition, we investigate the Gaussian splatting on the voxel space for faster rendering compared with the previous volume rendering

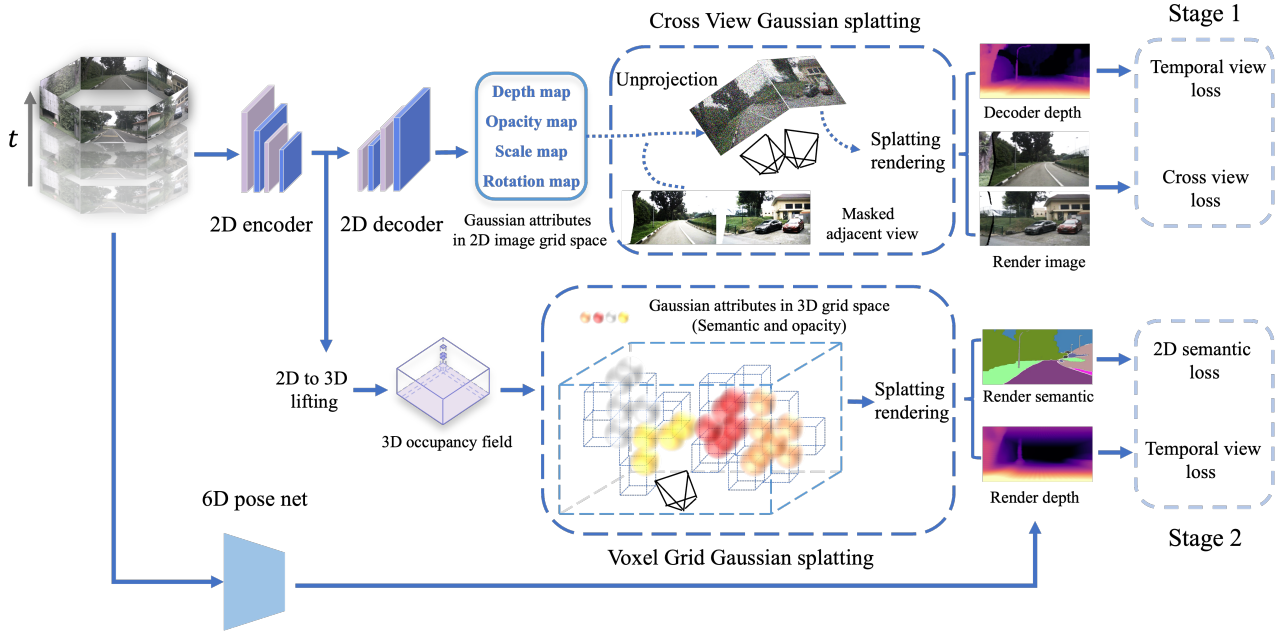


Figure 2. GaussianOcc is a two-stage method. In Stage 1, we train a scale-aware 6D pose network, using a U-Net architecture to predict Gaussian attributes in the 2D image grid space for cross-view Gaussian splatting. This approach provides scale information in the joint training with the 6D pose network. Based on the 6D pose from Stage 1, we perform self-supervised 3D occupancy estimation in Stage 2, where we lift the 2D features to a 3D voxel space and propose voxel grid Gaussian splatting for fast rendering. Note that, for clarity, we omit the line from the 6D pose network to the loss in Stage 1, and the 2D encoder is independent for each stage (not shared).

based works [11, 23, 54].

Note that, two recent works, GaussianFormer [24] and GaussianBeV [6], are closely related to ours in their focus on 3D occupancy estimation and BEV prediction. However, our exploration diverges by focusing on two new properties that Gaussian splatting can contribute to occupancy estimation: scale-aware training and faster rendering.

3. Method

3.1. Preliminaries

3D Gaussian splatting [26] is for modeling static 3D scenes using point primitives, where each primitive is characterized with the following attributes: (1) a 3D position $\mathcal{X} \in \mathbb{R}^3$, (2) a color defined by SH coefficients $c \in \mathbb{R}^k$ (where k denotes the dimensionality of the SH basis), (3) a rotation represented by a quaternion $r \in \mathbb{R}^4$, (4) a scaling factor $s \in \mathbb{R}_+^3$, and (5) an opacity $\alpha \in [0, 1]$. The original Gaussian splatting is for scene-specific, fast 3D novel view synthesis, where the attributes of Gaussian points are optimized by the multi-view constraint. In contrast, in this work, we explore a setting where Gaussian attributes are well-aligned in both 2D and 3D grids, allowing us to benefit from the Gaussian splatting rendering for the scale-aware training by cross-view constraint and faster rendering on voxel grids as illustrated in Figure 2.

3.2. Scale-aware training by Gaussian Splatting

Scale from spatial camera rig: Similar to the previous work [15, 27, 44], the scale information is from the surround camera rig. Specifically, the real-world scale can be obtained by leveraging camera extrinsic matrices which is to use spatial photometric loss in the overlap region between two adjacent views, *i.e.*, warping I_t^i to I_t^j :

$$p_t^{i \rightarrow j} = K^j(T^j)^{-1}T^i D_t^i(K^i)^{-1} p_t^i \quad (1)$$

where K^i, T^i are the intrinsic and extrinsic matrices of i -th camera, D_t^i is the predicted depth map of i -th camera, p_t is the corresponding pixel during the warping. The warping operation is achieved by bilinear interpolation with the corresponding $p_t^{i \rightarrow j}$. However, as pointed out by [44], the mapping $p_t^{i \rightarrow j}$ can easily go out of image bounds with the weak supervision signal in such a small overlap region. Therefore, apart from the spatial loss, [44] proposes to facilitate the Structure-from-Motion (SfM) to extract sparse depth information for the direct depth supervision to provide a stronger supervision signal, but it is time-consuming and not straightforward. Different from [44], [27] enhances the depth estimation performance with spatio-temporal context that does not need the sparse depth from SfM but the performance is still limited. Inspired by the explicit sparse depth supervision in [44], we ask whether we can enforce

the cross-view constraint on adjacent views more explicitly. The answer is yes. We find that the nature of Gaussian splatting is scale-aware projection that could serve for the cross-view stereo constraint. We propose Gaussian splatting for projection in stage 1 for better scale-aware training.

Gaussian Splatting for Projection (GSP): As illustrated in Figure 2, we adapt a depth network [52] to predict the Gaussian attributes in 2D grid space, where, apart from the original depth map, we also predict the scale map and rotation map. For each adjacent view, we first calculate the mask in the overlap region, then mask out one side of these overlap regions. Due to the presence of the other side’s overlap region, the unprojected 3D scene remains complete, which is critical for providing scale training, as indicated in the experiment section (Table 3). We then perform splatting rendering on the adjacent views to obtain the rendered image. If the depth map is accurately learned, the rendered image should resemble the original images, providing the necessary scale information for the entire pipeline.

The process of acquiring the overlap mask is illustrated in Figure 3. The acquisition of the overlap mask is similar to volume rendering. We densely sample points along the ray in one view, and a pixel is considered part of the overlap region if more than one sampled 3D point falls within the adjacent view. The overlap mask is determined by the camera extrinsic and defined max depth (e.g., 80m in nuScenes). Note that in the DDAD dataset [13], we exclude regions with self-occlusion (such as parts of the vehicle body). Finally, we apply an erosion operation from OpenCV library [2] to the mask for purification.

3.3. Fast rendering by Gaussian Splatting

Inefficient performance in volume rendering: For 2D supervision (semantic and depth maps), previous methods [11, 23, 37, 54] employed volume rendering based on dense sampling. Although the final 3D voxel representation for modeling the 3D scene is much quicker than the original implicit representation [35], it remains time-consuming, particularly when incorporating semantic map rendering. For example, in OccNeRF [54], the number of sampled points at a resolution of 180×320 is 108,735,066. However, the target optimized points correspond to the vertices in the 3D voxel grid, which total $320 \times 320 \times 24 = 2,577,525$. This redundancy in densely sampled points helps optimization with volume rendering but is highly inefficient.

Gaussian Splatting from Voxel (GSV): As analyzed above, the target optimized points are the vertices in the 3D voxel grid, prompting us to consider directly optimizing these vertices. Interestingly, we find that it is suitable to use the Gaussian splatting to replace the volume rendering if we regard the vertices of each the voxel grid as the position of the 3D Gaussian. Then, we can optimize the attributes of the 3D Gaussian, such as semantic and opacity information.

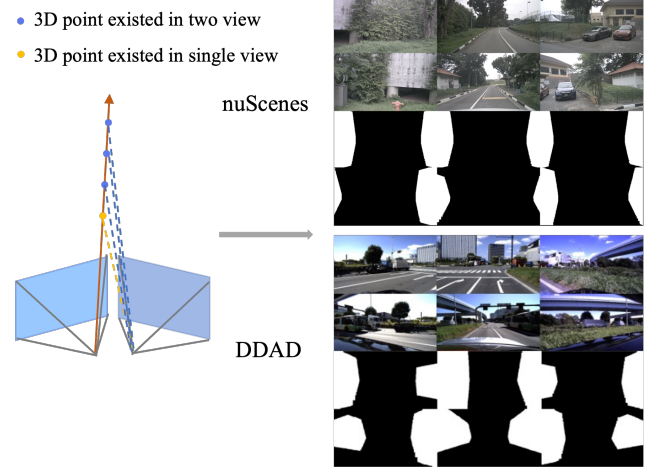


Figure 3. Overlap mask in nuScenes [3] and DDAD [13].

For example, in the empty space of the voxel, even though we have the vertices at that region during the splatting rendering, after the optimization, the network would predict the opacity as zero at these vertices then these vertices would not contribute any geometry or semantic information during the rendering. Since all the vertices are arranged in 3D voxel space with real-world 3D position \mathcal{X} , we use fixed scale s and fixed rotation r for each vertex for simplification. This allows us to model the 3D scene by optimizing the rest Gaussian attributes (semantic and opacity).

3.4. Loss function

We formulate the loss function of each stage as follows:

$$\mathcal{L}_{stage1} = \mathcal{L}_{temporal} + \mathcal{L}_{cross}, \quad (2)$$

$$\mathcal{L}_{stage2} = \mathcal{L}_{temporal} + \mathcal{L}_{semantic}, \quad (3)$$

$$(\mathcal{L}_{temporal}, \mathcal{L}_{cross}) = \frac{1 - SSIM(I_t, \hat{I}_t)}{2} + (\beta) \|I_t - \hat{I}_t\|, \quad (4)$$

where I_t and \hat{I}_t refer to the target image and the corresponding synthesized image, respectively. Note that \hat{I}_t in the temporal-view photometric loss $\mathcal{L}_{temporal}$ is generated by projecting pixels from the source image using the coordinate index. In contrast, \hat{I}_t in the cross-view photometric loss \mathcal{L}_{cross} is derived from our proposed cross-view Gaussian splatting method. $\mathcal{L}_{semantic}$ is 2D semantic loss. The β is set to 0.15 to balance the two loss terms. For $\mathcal{L}_{temporal}$ and $\mathcal{L}_{semantic}$, we recommend [54] for further details.

4. Experiment

4.1. Tasks, datasets, and metric

nuScenes [3]: For 3D occupancy estimation, we utilize annotations from Occ3D-nuScenes [41], which includes 600

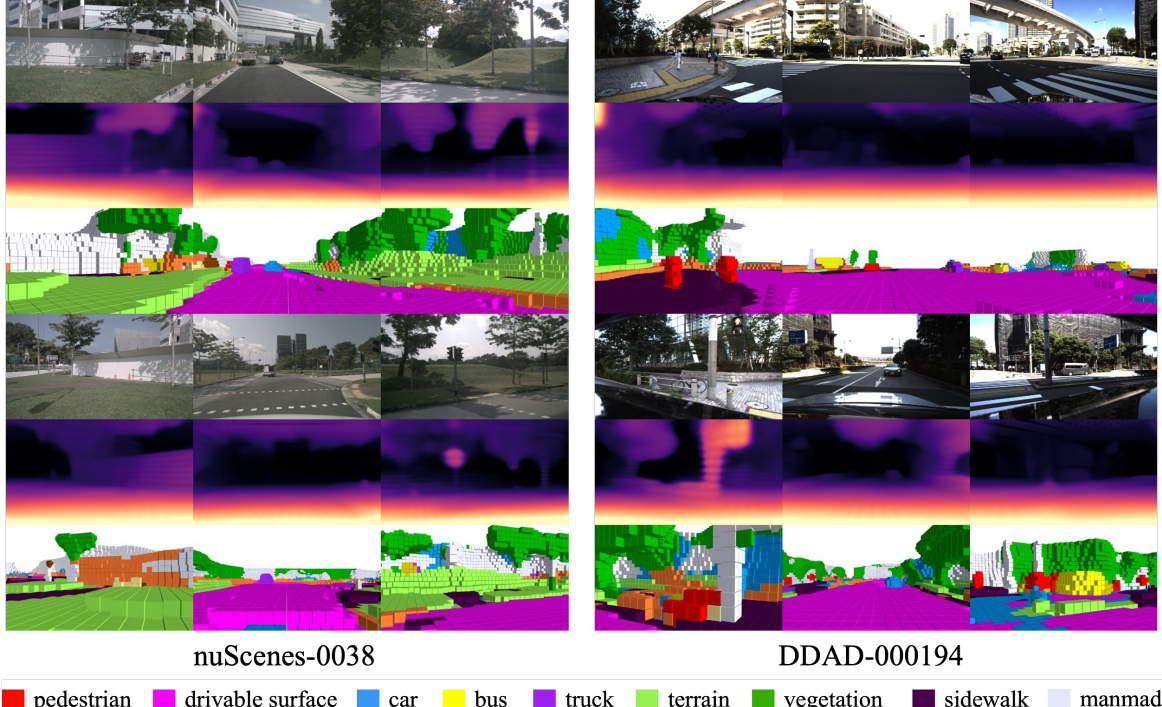


Figure 4. Visualization of the render depth map and 3D occupancy prediction on the nuScenes and DDAD datasets.

Method	GT Occ.	GT Pose	mIoU*	mIoU
MonoScene [4]	✓	✗	6.33	6.06
BEVDet [20]	✓	✗	20.03	19.38
BEVFormer [29]	✓	✗	24.64	23.67
OccFormer [56]	✓	✗	22.39	21.93
RenderOcc [37]	✓	✗	24.53	23.93
TPVFormer [22]	✓	✗	28.69	27.83
CTF-Occ [41]	✓	✗	29.54	28.53
SimpleOcc [11]	✗	✓	7.99	7.05
SelfOcc [23]	✗	✓	10.54	9.30
OccNeRF [54]	✗	✓	10.81	9.54
GaussianOcc	✗	✗	11.26	9.94

Table 1. 3D occupancy prediction performance on the Occ3D-nuScenes dataset in mIoU metric. Since ‘other’ and ‘other flat’ classes are the invalid prompts for open-vocabulary models, we also calculate ‘mIoU*’ as the result ignoring the classes that do not consider these two classes during evaluation, while ‘mIoU’ is the original result. GT Occ. means using the ground truth occupancy label for the supervision. GT Pose is the ground truth pose from the sensor for self-supervised geometry learning. The full table is placed in the supplementary material with each category result.

scenes for training and 150 scenes for evaluation. Each sample has a perception range of [-40m, -40m, -1m, 40m, 40m, 5.4m] with a voxel size of 0.4m. For fair comparison, we use the 2D semantic map provided by OccNeRF [54].

We measure 3D occupancy estimation performance using the mean Intersection over Union (mIoU) metric. For depth estimation, we set the perception range in [-80m, -80m, -1m, 80m, 80m, 6m], while we clamp the ground truth to a range of 0.1m to 80m for evaluation, consistent with OccNeRF and SurroundDepth [44]. We evaluate depth maps using error metrics (Abs Rel, Sq Rel, RMSE, RMSE log) and threshold accuracy metrics (δ).

DDAD [13]: Due to the lack of ground truth labels, we only present qualitative results for the fully self-supervised 3D occupancy estimation setting. Following the procedure on the nuScenes dataset, we obtain the 2D semantic labels according to the OccNeRF pipeline. For depth estimation, we also set the perception range in [-80m, -80m, -1m, 80m, 80m, 6m], but clamp the ground truth to a range of 0.1m to 200m for evaluation, consistent with SurroundDepth [44].

4.2. Implementation details

Network details: For U-Net architecture, we adapt New-CRFs [52] to predict the Gaussian attributes, which is based on the Swin Transformer [33]. The 6D pose network is the same as that used in SurroundDepth [44]. For the 2D-to-3D lifting, we follow the approach used in SimpleOcc [11]. In the depth estimation benchmark, we use the network proposed by SimpleOcc, where the final output size is 256×256×16. In our Gaussian splatting setting, we further upsample the final output to 512×512×32 for improved performance since we observe that a finer voxel grid leads to

Method	<i>GT pose</i>	<i>Occ.</i>	Abs Rel	Sq Rel	RMSE	RMSE log	$\delta < 1.25$	$\delta < 1.25^2$	$\delta < 1.25^3$
nuScenes [3]									
FSM [15]	✗	✗	0.297	-	-	-	-	-	-
FSM* [15]	✗	✗	0.319	7.534	7.860	0.362	0.716	0.874	0.931
SurroundDepth [44]	✗	✗	0.280	4.401	7.467	0.364	0.661	0.844	0.917
SA-FSM [50]	✗	✗	0.272	4.706	7.391	0.355	0.689	0.868	0.929
VFF [27]	✗	✗	0.289	5.718	7.551	0.348	0.709	0.876	0.932
R3D3 [38]	✗	✗	0.253	4.759	7.150	-	0.729	-	-
GaussianOcc \ddagger	✗	✗	0.258	5.733	7.222	0.343	0.753	0.888	0.934
SimpleOcc [11]	✓	✓	0.224	3.383	7.165	0.333	0.753	0.877	0.930
OccNeRF [54]	✓	✓	0.202	2.883	6.697	0.319	0.768	0.882	0.931
OccNeRF [54] \dagger	✓	✓	0.456	12.682	9.194	0.399	0.704	0.833	0.890
SelfOcc [23]	✓	✓	0.215	2.743	6.706	0.316	0.753	0.875	0.932
GaussianOcc	✗	✓	0.211	3.115	7.131	0.326	0.762	0.878	0.931
GaussianOcc \dagger	✗	✓	0.197	1.846	6.733	0.312	0.746	0.873	0.931
DDAD [13]									
FSM* [15]	✗	✗	0.228	4.409	13.433	0.342	0.687	0.870	0.932
VFF [27]	✗	✗	0.218	3.660	13.327	0.339	0.674	0.862	0.932
SurroundDepth [44]	✗	✗	0.208	3.371	12.977	0.330	0.693	0.871	0.934
SA-FSM [50]	✗	✗	0.187	3.093	12.578	0.311	0.731	0.891	0.945
R3D3 [38]	✗	✗	0.162	3.019	11.408	-	0.811	-	-
GaussianOcc \ddagger	✗	✗	0.212	3.556	12.564	0.320	0.701	0.888	0.944
GaussianOcc	✗	✓	0.228	3.854	14.326	0.357	0.660	0.853	0.922

Table 2. Comparisons for self-supervised multi-camera depth estimation on the nuScenes [3] and DDAD datasets [13]. The results are averaged over all views without median scaling at test time. ‘FSM*’ is the reproduced result in [27]. GaussianOcc \ddagger represents the depth estimation result from Stage 1. GaussianOcc \dagger and OccNeRF \dagger means the model trained with the semantic information. *Occ.* represents the ability of the method to predict the 3D occupancy.

Scale-aware training in [27, 44]		Scale-aware training by ours				Abs Rel	Sq Rel	RMSE	RMSE log	$\delta < 1.25$	$\delta < 1.25^2$	$\delta < 1.25^3$
<i>Loss in [44]</i>	<i>Loss in [27]</i>	<i>GS loss</i>	<i>Mask</i>	<i>Erode</i>	<i>Refine</i>							
✓*	✓					0.280	4.401	7.467	0.364	0.661	0.844	0.917
						0.672	25.405	11.999	0.568	0.419	0.808	0.878
						0.289	5.718	7.551	0.348	0.709	0.876	0.932
						0.285	6.046	7.514	0.342	0.702	0.865	0.931
		✓	✓	✓	✓	0.798	11.571	15.251	1.472	0.006	0.015	0.028
						0.293	7.127	7.536	0.376	0.743	0.876	0.923
						0.281	6.986	7.347	0.354	0.766	0.885	0.929
						0.258	5.733	7.222	0.343	0.753	0.888	0.934

Table 3. Ablation study for scale-aware depth estimation on the nuScenes dataset [14]. ✓* means the result from the original paper and ✓ means the result using New-CRFs [52] as the depth network the same as ours. *GS loss* means using the spatial context constraint by our proposed Gaussian splatting for projection. *Mask* represents using the mask-out strategy before the unprojection. *Erode* means the erode process to the binary overlap mask and *Refine* is the refinement of depth estimation network with 2 epochs by fixing the 6D pose network.

a finer rendered depth map, which requires ignorable computational cost. For occupancy estimation, we use the same network as OccNeRF [54] to ensure a fair comparison.

Training details: We propose a two-stage training process for fully self-supervised 3D occupancy estimation. In stage 1, we jointly train the depth estimation network and the 6D pose network, where we train the models for 8 epochs on the nuScenes dataset and 12 epochs on the DDAD dataset. In stage 2, we train the 3D occupancy network in a self-supervised manner with the 6D pose predicted from stage 1 rather than the ground truth pose used in OccNeRF [54]. We train the models for 12 epochs on both the nuScenes and

DDAD datasets. The optimizer and learning rate adjustment strategy follow those used in SimpleOcc [11] and OccNeRF [54]. More implementation details (including code) are provided in the supplementary material.

4.3. Main results

3D occupancy estimation in nuScenes: As shown in Table 1, the proposed GaussianOcc achieves the best performance compared to other self-supervised methods. In particular, we do not require ground truth occupancy labels and ground truth 6D poses for training, thanks to the predicted 6D pose from the stage 1. In addition, we also achieve the

good result on the RayIoU metric [31], with further details provided in the supplementary material.

3D occupancy estimation in DDAD: Thanks to our fully self-supervised learning setting, we are able to perform 3D occupancy estimation on the DDAD dataset [13]. To the best of our knowledge, our work is the first to introduce 3D occupancy estimation on this dataset, although we cannot provide quantitative results due to the lack of 3D occupancy label. We present visualization results in Figure 4. More results can be found in the supplementary material.

Depth estimation: We present a comparison of depth estimation results in Table 2 for both the nuScenes and DDAD datasets. In stage 1, GaussianOcc \ddagger achieves top performance on the nuScenes dataset and delivers competitive results on the DDAD dataset. It is important to note that methods such as SurroundDepth [44] and SA-FSM [50] rely on third-party module for the sparse depth supervision. Additionally, SA-FSM is preprint work and has not released the code. R3D3 [38] is a temporal offline refinement method that requires multi-frame optimization, as discussed in [23]. In stage 2, which involves depth estimation from rendering, our method also achieves competitive results compared to those trained with ground truth poses. Besides, we observe that the rendered depth in stage two outperforms the depth results from stage 1 on the nuScenes dataset, whereas the opposite is true for the DDAD dataset. This discrepancy might be attributed to differences in perception range—80 meters in nuScenes versus 200 meters in DDAD. Moreover, an interesting phenomenon is that the semantic information is helpful for the depth estimation as indicated in GaussianOcc \dagger whereas it worsens the result in OccNeRF \dagger . This shows the difference between the Gaussian splatting rendering and volume rendering.

4.4. Ablation Study

Scale-aware training: To demonstrate the effectiveness of the proposed scale-aware training using Gaussian Splatting, we conducted experiments comparing our method with existing approaches [27, 44] on Table 3. For a more fair comparison, we also implemented scale-aware training on [27, 44] that uses the same depth estimation network as ours [52], noted as \checkmark . We could reproduce the result on [27], but it is not good to train network with the sparse depth following [44]. Our proposed scale-aware training method is better than [27, 44]. Specifically, we observed that a naive implementation of Gaussian splatting without a masking strategy for cross-view rendering is ineffective because it would lead to a sub-optimal solution that the rendered image is still from the current view. Besides, to enhance performance, we introduced an erosion operation on the binary mask to purify it, excluding regions that may fall outside the overlap area. This step ensures better alignment during training. Finally, we refined the depth estimation

by fixing the 6D pose network and disabling the cross-view loss. This refinement helps reduce artifacts at the edges of the overlap region. We present the cross-view splatting render result in Figure 5, where the rendering result in overlap regions is reasonable in the correct depth estimation from cross view that verifies our design.

6D pose learning and training strategy: Considering the GT pose from the sensor is imperfect as a lack of vertical movement [36]. We further evaluate the learned 6D pose quality by the self-supervised depth result at stage 2, where the experiments on Table 4 use the same network but with different pose constraints. Our result is competitive compared with GT pose, indicating that the predicted pose is of high quality. Furthermore, one stage training was ineffective in using the 6D pose from the jointly trained with 6D pose network because the cross-view loss in the 3D voxel space led to local optimization, which failed to generalize predictions to non-overlapping regions., as shown in Figure 6. However, this issue did not arise in the depth maps generated by the 2D decoder in stage 1, which is why we need the two-stage training process. Besides, our result is also better than [27], which is consistent the depth result on Table 3.

Volume rendering and Splatting rendering: In Table 5, we compare the performance of volume rendering (VR) and splatting rendering (SR) in the voxel space. For each 3D Gaussian, we set a uniform scale s for all Gaussians, considering the well-arranged positions of vertices within the voxel grid. Since the scale s is consistent across all three dimensions, we set the rotation \mathbf{R} as the identity matrix. We first explored the optimal scale and found that a scale of 0.1 produced the best results. Notably, the performance of VR and SR was very close when using this scale. The render depth maps are shown in Figure 6. The depth map by the volume rendering is smoother thanks to dense sampling and the depth maps from splatting rendering have the graininess effect, especially at the small scale factor.

Pose and render types ablation study in occupancy task: In Table 6, we present an ablation study to evaluate the impact of using ground truth versus learned poses in the occupancy task, with training conducted using different rendering methods. The results show that splatting rendering achieves superior performance in both occupancy metrics (mIoU*) and depth metrics. One observation is that depth estimation results with the semantic learning in volume rendering are significantly worse than those in Table 2 whereas the proposed splatting rendering method maintains consistent performance, which suggests the splatting rendering in voxel grid contributes better 3D geometry.

Rendering efficiency analysis: We analyze rendering efficiency in Table 7. The results show that volume rendering consumes 5 times more rendering time compared to splatting rendering. As resolution increases, both volume rendering time and GPU consumption rise significantly. In

Pose type	Abs Rel	Sq Rel	RMSE	$\delta < 1.25$
GT pose	0.214	3.362	7.127	0.771
One stage training	0.946	17.008	16.397	0.103
[27]	0.235	3.592	7.295	0.750
Ours	0.211	3.115	7.131	0.762

Table 4. Comparison of pose type for stage 2 training on depth estimation task [14]. One stage training directly uses the cross-view loss to the rendered depth map. Apart from the GT pose, we also experiment the learned pose from [27] for comparison.

Render type	Abs Rel	Sq Rel	RMSE	$\delta < 1.25$
VR	0.215	3.508	7.113	0.775
SR ($s = 0.05$)	0.223	3.694	7.246	0.761
SR ($s = 0.1$)	<u>0.217</u>	<u>3.504</u>	<u>7.152</u>	<u>0.770</u>
SR ($s = 0.15$)	<u>0.217</u>	3.406	7.204	0.763

Table 5. Comparison of the render result between the volume rendering (VR) [54] and splatting rendering (SR, Ours) on depth estimation task [14]. The coefficient s means the scale of the 3D Gaussian. We use GT pose for this set of the ablation study.

Pose type	mIoU*	Abs Rel	Sq Rel	$\delta < 1.25$
GT pose (VR)	10.81	0.456	12.682	0.704
GT pose (SR)	11.30	0.225	4.339	0.787
Learned pose (VR)	11.19	0.506	15.577	0.684
Learned pose (SR)	11.26	0.197	1.846	0.746

Table 6. Comparison of ground truth pose (GT Pose) and our learned pose (Two stages) on 3D occupancy estimation task [14] in volume rendering (VR) and splatting rendering (SR).

contrast, splatting rendering shows no significant increase in computational cost with higher resolutions, highlighting its efficiency and scalability.

Bonus of the fully self-supervised setting: The fully self-supervised setting of our method could be a general pre-training solution for supervised learning. After the self-supervised training on the DDAD and nuScenes datasets, we further finetune the model with the 3D occupancy label from Occ3D-nuScenes [41]. As shown in Table 8, experiments with self-supervised pretraining outperform the baseline. In particular, we find that pretraining on nuScenes is better than the DDAD dataset, which may own to the domain gap factors, such as differences in the scenarios (RGB images) and sensor configurations (camera extrinsics).

5. Conclusion

In this paper, we introduce GaussianOcc, a fully self-supervised and efficient method for 3D occupancy estimation. Through the carefully designed cross-view splatting rendering, we can accurately learn the real scale in depth and the 6D pose, enabling effective self-supervised 3D occupancy learning. Additionally, the proposed Gaussian splatting in voxel grids outperforms volume rendering

Render type	Render resolution and time (s)			Training time (h)
	180 × 320	240 × 520	360 × 640	
VR	≈ 0.85	≈ 1.57	N/A	≈ 2.68
SR	≈ 0.17	≈ 0.17	≈ 0.17	≈ 1

Table 7. Comparison of rendering efficiency between volume rendering (VR) [54] and splatting rendering (SR, Ours) on 3D occupancy estimation task [14]. The render time is calculated from surround 6 images. "N/A" indicates out-of-memory errors running in NVIDIA A 100 (40 GB). Training time is averaged per epoch.

Method	Pretraining setting	mIoU
Baseline	None	37.29
Self-supervised pretraining	DDAD nuScenes	37.40 38.45

Table 8. The study on SimpleOcc [11] with fully self-supervised pretraining. The baseline is directly training the model with 3D occupancy labels. The self-supervised pretraining is conducted on DDAD and nuScenes and then finetuned the model with 3D occupancy label. The number with bold typeface means the best.

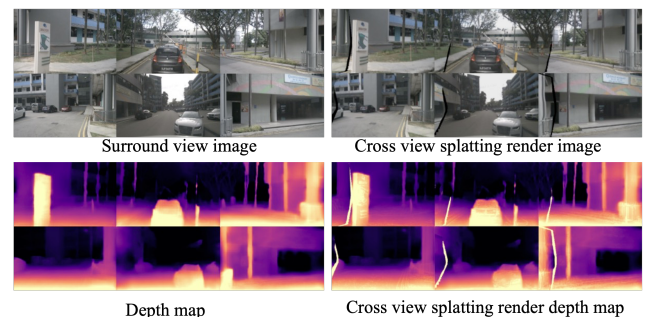


Figure 5. **Visualization of the depth map, splatting render image and depth map from cross view in stage 1.**

in 3D occupancy estimation while reducing computational cost. As a bonus, the fully self-supervised setting of the proposed method could serve as the general pretrain solution to enhance the 3D occupancy estimation performance. We validate our method on the nuScenes and DDAD datasets, demonstrating its strong generalization ability to surround view scenes.

Abstract

In this supplementary material, we provide more implementation details, experiment results, and further discussion on the limitations and future work.

6. More implementation details

The detailed parameter setting in Gaussian attributes estimation network [52]. During the joint depth and 6D

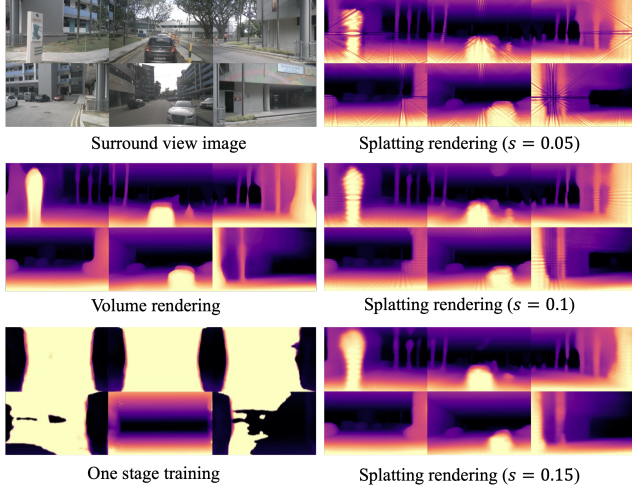


Figure 6. The comparison for the depth map in the different setting, corresponding to the training strategy in Table 4 and rendering type in Table 5.

pose training in stage 1, we predict the 3D Gaussian parameters alongside the 2D depth map. Since the Gaussian parameters are well-arranged in the 2D image plane prior to unprojection, we maintain equal scaling across all three dimensions of each 3D Gaussian and constrain the maximum scale to 0.02. Given that the scale s is uniform across all dimensions, we set the rotation matrix \mathbf{R} to the identity matrix. Additionally, we assign an opacity value of 1 to each 3D Gaussian, ensuring that every 2D depth value corresponds to a valid point in 3D space. We do not predict the color defined by SH coefficients c , while we directly use the source RGB image as the color map the same as in [57].

The detailed parameter setting in voxel grid splatting rendering. We chose a fixed scale for each grid vertex to ensure a well-arranged structure that accurately models the 3D space. If we use a learnable scale, it may lead to a situation where the scale is small but the opacity is large, which may not be captured in the rendered depth map and semantic map but could still affect the 3D occupancy result. Therefore, using a fixed scale is simple and sufficient for optimization, as demonstrated in the results presented in the main paper. Since the scale $s \in \mathbb{R}_+^3$ are identical for both three dimensions, we do not need to predict the rotation $r \in \mathbb{R}^4$ and set it with the identical matrix is sufficient. Similar to the OccNeRF [54], we render the 2D feature map for the semantic regression, while we leverage the 3D Gaussian splatting rendering and OccNeRF uses volume rendering.

The detailed parameter setting in training. We follow the training setting as OccNeRF [54], the resolution of input images and rendered depth maps are set as 384×640 and 180×320 respectively. All experiments are conducted on 8

NVIDIA A100 (40 GB).

The detailed training strategy of the self-supervised pretraining setting. We first do the self-supervised training with 12 epochs with the learned pose from stage 1 and the 2D pseudo semantic label, which does not require the 3D occupancy label. Then, we finetune the model with 12 epochs with the 3D occupancy label. We add the RayIoU metric [31] in Table 11 for a comprehensive comparison.

The detailed definition of depth map metric. Following the depth estimation task [44], we report the depth map evaluation with the following metrics,

$$\begin{aligned}
 \text{Abs Rel: } & \frac{1}{|M|} \sum_{d \in M} |\hat{d} - d^*| / d^*, \\
 \text{Sq Rel: } & \frac{1}{|M|} \sum_{d \in M} \|\hat{d} - d^*\|^2 / d^*, \\
 \text{RMSE: } & \sqrt{\frac{1}{|M|} \sum_{d \in M} \|\hat{d} - d^*\|^2}, \\
 \text{RMSE log: } & \sqrt{\frac{1}{|M|} \sum_{d \in M} \|\log \hat{d} - \log d^*\|^2}, \\
 \delta < t : \% \text{ of } d \text{ s.t. } \max \left(\frac{\hat{d}}{d^*}, \frac{d^*}{\hat{d}} \right) & = \delta < t,
 \end{aligned} \tag{5}$$

where M is the valid pixel, \hat{d} is the ground truth depth and d^* is the predicted depth.

7. More experiment results

mIoU metric. Due to the limited space in the main paper, the full table of mIoU results is presented in Table 9 for reference.

RayIoU metric. In addition to the mIoU metric for 3D occupancy estimation, we also evaluate our method with a novel metric, RayIoU, introduced by the recent work [31]. The RayIoU is a ray-based evaluation metric that resolves the inconsistency penalty along the depth axis introduced in the traditional voxel-level mIoU criteria. As shown in Table 10, our approach also outperforms OccNeRF [54] in this metric as well. It's important to note that the FPS is calculated excluding rendering time. Since GaussianOcc and OccNeRF utilize the same network architecture, they share the same inference time when the rendering process is not taken into account.

More visualization. We provide more visualization for nuScenes dataset in Figure 7 and DDAD dataset in Figure 8. Please check the attached videos for sequence visualization.

More analysis on different supervision types. In Figure 9, we present visualizations of different supervision types. These visualizations highlight key differences in the results for the invisible regions (marked with red rectangles)

and the rendered depth quality (marked with green rectangles).

Experiments (1) and (2) involve supervision using ground truth (GT) occupancy labels. Specifically:

Experiment (1) is trained without the visible mask provided by Occ3D-nuScenes [41], which defines the visibility of the occupancy labels. Without this mask, the invisible regions are treated as empty, and the loss function is applied to these regions as well. Experiment (2), on the other hand, excludes the loss computation in invisible regions. From the results, we observe that in Experiment (1), the model tends to predict empty values for invisible regions due to empty loss penalty. In contrast, Experiment (2), by ignoring the loss in invisible areas, shows more non-empty predictions in these regions.

Self-supervised experiments (3) and (4) rely on rendering techniques, which inherently cannot optimize predictions in invisible regions. This limitation leads to non-empty predictions in the red-highlighted areas. Notably, Experiment (4) frequently predicts invisible regions as related to foreground categories, as shown in the dark rectangles. Conversely, Experiment (3) demonstrates a consistent tendency to classify invisible regions as man-made structures, likely because the surrounding environment predominantly consists of man-made elements.

Additionally, the depth maps in the green-highlighted areas show that our Gaussian splatting rendering produces higher-quality depth predictions compared to volume rendering, consistent with the quantitative results in Table 6 of the main paper. Since Experiments (1) and (2) do not involve rendering-based training, they fail to produce reasonable depth predictions.

8. Limitation and future work

The proposed method achieves reasonable predictions in most scenes; however, we observe that some cases still present challenges, as shown in Figure 10. Specifically, in the DDAD dataset, incorrect predictions occur in the back camera in certain situations as marked with the red circle, where the drivable surface is mistakenly projected into the car due to extensive self-occlusion. Notably, this issue is absent in the nuScenes dataset, which has less self-occlusion. We believe that this problem could be mitigated with better 2D semantic maps for supervision, which warrants further investigation. The proposed method is for the surround view setting which is not suitable for the monocular images and the two-stage training procedure is a little bit time-consuming. Therefore, in the future, we will further investigate to apply the proposed method for one-stage training. Additionally, in stage 1, we leverage the spatial cross-view constraint through the proposed Gaussian splatting method. In the future, we aim to explore its potential benefits for temporal view synthesis as well.

References

- [1] Yanqi Bao, Tianyu Ding, Jing Huo, Yaoli Liu, Yuxin Li, Wenbin Li, Yang Gao, and Jiebo Luo. 3d gaussian splatting: Survey, technologies, challenges, and opportunities. *arXiv preprint arXiv:2407.17418*, 2024. [2](#)
- [2] Gary Bradski. The opencv library. *Dr. Dobb's Journal: Software Tools for the Professional Programmer*, 25(11):120–123, 2000. [4](#)
- [3] Holger Caesar, Varun Bankiti, Alex H Lang, Sourabh Vora, Venice Erin Lioung, Qiang Xu, Anush Krishnan, Yu Pan, Giancarlo Baldan, and Oscar Beijbom. nuscenes: A multimodal dataset for autonomous driving. In *CVPR*, pages 11621–11631, 2020. [2, 4, 6](#)
- [4] Anh-Quan Cao and Raoul de Charette. Monoscene: Monocular 3d semantic scene completion. In *CVPR*, pages 3991–4001, 2022. [5, 11](#)
- [5] Anh-Quan Cao and Raoul de Charette. Scenerf: Self-supervised monocular 3d scene reconstruction with radiance fields. In *ICCV*, pages 9387–9398, 2023. [1](#)
- [6] Florian Chabot, Nicolas Granger, and Guillaume Lapouge. Gaussianbev: 3d gaussian representation meets perception models for bev segmentation. *arXiv preprint arXiv:2407.14108*, 2024. [3](#)
- [7] David Charatan, Sizhe Lester Li, Andrea Tagliasacchi, and Vincent Sitzmann. pixelsplat: 3d gaussian splats from image pairs for scalable generalizable 3d reconstruction. In *Proceedings of the IEEE/CVF Conference on Computer Vision and Pattern Recognition*, pages 19457–19467, 2024. [2](#)
- [8] Yuanxing Duan, Fangyin Wei, Qiyu Dai, Yuhang He, Wenzheng Chen, and Baoquan Chen. 4d-rotor gaussian splatting: Towards efficient novel view synthesis for dynamic scenes. In *ACM SIGGRAPH 2024 Conference Papers*, pages 1–11, 2024. [2](#)
- [9] Shaoheng Fang, Zi Wang, Yiqi Zhong, Junhao Ge, and Si-heng Chen. Tbp-former: Learning temporal bird’s-eye-view pyramid for joint perception and prediction in vision-centric autonomous driving. In *Proceedings of the IEEE/CVF Conference on Computer Vision and Pattern Recognition*, pages 1368–1378, 2023. [1](#)
- [10] Wanshui Gan, Hongbin Xu, Yi Huang, Shifeng Chen, and Naoto Yokoya. V4d: Voxel for 4d novel view synthesis. *IEEE Transactions on Visualization and Computer Graphics*, 2023. [1, 2](#)
- [11] Wanshui Gan, Ningkai Mo, Hongbin Xu, and Naoto Yokoya. A comprehensive framework for 3d occupancy estimation in autonomous driving. *IEEE Transactions on Intelligent Vehicles*, 2024. [1, 2, 3, 4, 5, 6, 8, 11, 15](#)
- [12] Clément Godard, Oisin Mac Aodha, Michael Firman, and Gabriel J Brostow. Digging into self-supervised monocular depth estimation. In *ICCV*, pages 3828–3838, 2019. [2](#)
- [13] Vitor Guizilini, Rares Ambrus, Sudeep Pillai, Allan Raventos, and Adrien Gaidon. 3d packing for self-supervised monocular depth estimation. In *Proceedings of the IEEE/CVF conference on computer vision and pattern recognition*, pages 2485–2494, 2020. [2, 4, 5, 6, 7](#)
- [14] Vitor Guizilini, Rares Ambrus, Sudeep Pillai, Allan Raventos, and Adrien Gaidon. 3d packing for self-supervised

Method	GT Occ. GT Pose																		
	mIoU*	mIoU	barrier	bicycle	bus	car	const. veh.	motorcycle	pedestrian	traffic cone	trailer	truck	drive. surf.	sidewalk	terrain	manmade	vegetation		
MonoScene [4]	✓	✗	6.33	6.06	7.23	4.26	4.93	9.38	5.67	3.98	3.01	5.90	4.45	7.17	14.91	7.92	7.43	1.01	7.65
BEVDet [20]	✓	✗	20.03	19.38	30.31	0.23	32.26	34.47	12.97	10.34	10.36	6.26	8.93	23.65	52.27	26.06	22.31	15.04	15.10
BEVFormer [29]	✓	✗	24.64	23.67	38.79	9.98	34.41	41.09	13.24	16.50	18.15	17.83	18.66	27.70	48.95	29.08	25.38	15.41	14.46
OccFormer [56]	✓	✗	22.39	21.93	30.29	12.32	34.40	39.17	14.44	16.45	17.22	9.27	13.90	26.36	50.99	34.66	22.73	6.76	6.97
RenderOcc [37]	✓	✗	24.53	23.93	27.56	14.36	19.91	20.56	11.96	12.42	12.14	14.34	20.81	18.94	68.85	42.01	43.94	17.36	22.61
TPVFormer [22]	✓	✗	28.69	27.83	38.90	13.67	40.78	45.90	17.23	19.99	18.85	14.30	26.69	34.17	55.65	37.55	30.70	19.40	16.78
CTF-Occ [41]	✓	✗	29.54	28.53	39.33	20.56	38.29	42.24	16.93	24.52	22.72	21.05	22.98	31.11	53.33	37.98	33.23	20.79	18.00
SimpleOcc [11]	✗	✓	7.99	7.05	0.67	1.18	3.21	7.63	1.02	0.26	1.80	0.26	1.07	2.81	40.44	18.30	17.01	13.42	10.84
SelfOcc [23]	✗	✓	10.54	9.30	0.15	0.66	5.46	12.54	0.00	0.80	2.10	0.00	0.00	8.25	55.49	26.30	26.54	14.22	5.60
OccNeRF [54]	✗	✓	10.81	9.54	0.83	0.82	5.13	12.49	3.50	0.23	3.10	1.84	0.52	3.90	52.62	20.81	24.75	18.45	13.19
GaussianOcc	✗	✗	11.26	9.94	1.79	5.82	14.58	13.55	1.30	2.82	7.95	9.76	0.56	9.61	44.59	20.10	17.58	8.61	10.29

Table 9. **3D occupancy prediction performance on the Occ3D-nuScenes dataset in mIoU metric.** Since ‘other’ and ‘other flat’ classes are the invalid prompts for open-vocabulary models, we also calculate ‘mIoU*’ as the result ignoring the classes that do not consider these two classes during evaluation, while ‘mIoU’ is the original result. GT Occ. refers to the use of the ground truth occupancy label for supervision. GT Pose is the ground truth pose from the sensor for self-supervised geometry learning.

Method	GT Occ. GT Pose		Backbone	Input Size	Epoch	RayIoU	RayIoU _{1m, 2m, 4m}			mIoU	FPS
	GT Occ.	GT Pose					RayIoU _{1m}	RayIoU _{2m}	RayIoU _{4m}		
BEVFormer (4f) [29]	✓	✗	R101	1600×900	24	32.4	26.1	32.9	38.0	39.2	3.0
RenderOcc [37]	✓	✗	Swin-B	1408×512	12	19.5	13.4	19.6	25.5	24.4	-
SimpleOcc [11]	✓	✗	R101	672×336	12	28.2	22.3	28.7	33.7	37.3	9.7
BEVDet-Occ (2f) [19]	✓	✗	R50	704×256	90	29.6	23.6	30.0	35.1	36.1	2.6
BEVDet-Occ-Long (8f)	✓	✗	R50	704×384	90	32.6	26.6	33.1	38.2	39.3	0.8
FB-Occ (16f) [30]	✓	✗	R50	704×256	90	33.5	26.7	34.1	39.7	39.1	10.3
SparseOcc (8f)	✓	✗	R50	704×256	24	34.0	28.0	34.7	39.4	30.1	17.3
SparseOcc (16f)	✓	✗	R50	704×256	48	36.1	30.2	36.8	41.2	30.9	12.5
OccNeRF [54]	✗	✓	R101	640×384	12	10.49	6.93	10.28	14.26	9.54	10.8
GaussianOcc	✗	✗	R101	640×384	12	11.85	8.69	11.90	14.95	9.94	10.8

Table 10. **3D Occupancy prediction performance on the Occ3D-nuScenes dataset in RayIoU metric.** GT Occ. means using the ground truth occupancy label for the supervision. GT Pose is the ground truth pose from the sensor for self-supervised geometry learning. “8f” and “16f” mean fusing temporal information from 8 or 16 frames. mIoU is the mean Intersection over Union for all categories. FPS means frame per second for each method, which is measured on a Tesla A100 GPU.

- monocular depth estimation. In *CVPR*, pages 2485–2494, 2020. [6, 8](#)
- [15] Vitor Guizilini, Igor Vasiljevic, Rares Ambrus, Greg Shakhnarovich, and Adrien Gaidon. Full surround monodepth from multiple cameras. *RAL*, 7(2):5397–5404, 2022. [2, 3, 6](#)
- [16] Xianda Guo, Wenjie Yuan, Yunpeng Zhang, Tian Yang, Chenming Zhang, Zheng Zhu, and Long Chen. A simple baseline for supervised surround-view depth estimation. *arXiv preprint arXiv:2303.07759*, 2023. [2](#)
- [17] Adrian Hayler, Felix Wimbauer, Dominik Muhle, Christian Rupprecht, and Daniel Cremers. S4c: Self-supervised semantic scene completion with neural fields. In *2024 International Conference on 3D Vision (3DV)*, pages 409–420. IEEE, 2024. [1](#)
- [18] Lei He, Leheng Li, Wenchao Sun, Zeyu Han, Yichen Liu, Sifa Zheng, Jianqiang Wang, and Keqiang Li. Neural radiance field in autonomous driving: A survey. *arXiv preprint arXiv:2404.13816*, 2024. [2](#)
- [19] Junjie Huang and Guan Huang. Bevdet4d: Exploit temporal cues in multi-camera 3d object detection. *arXiv preprint arXiv:2203.17054*, 2022. [11](#)
- [20] Junjie Huang, Guan Huang, Zheng Zhu, and Dalong Du. Bevdet: High-performance multi-camera 3d object detection in bird-eye-view. *arXiv preprint arXiv:2112.11790*, 2021. [5, 11](#)

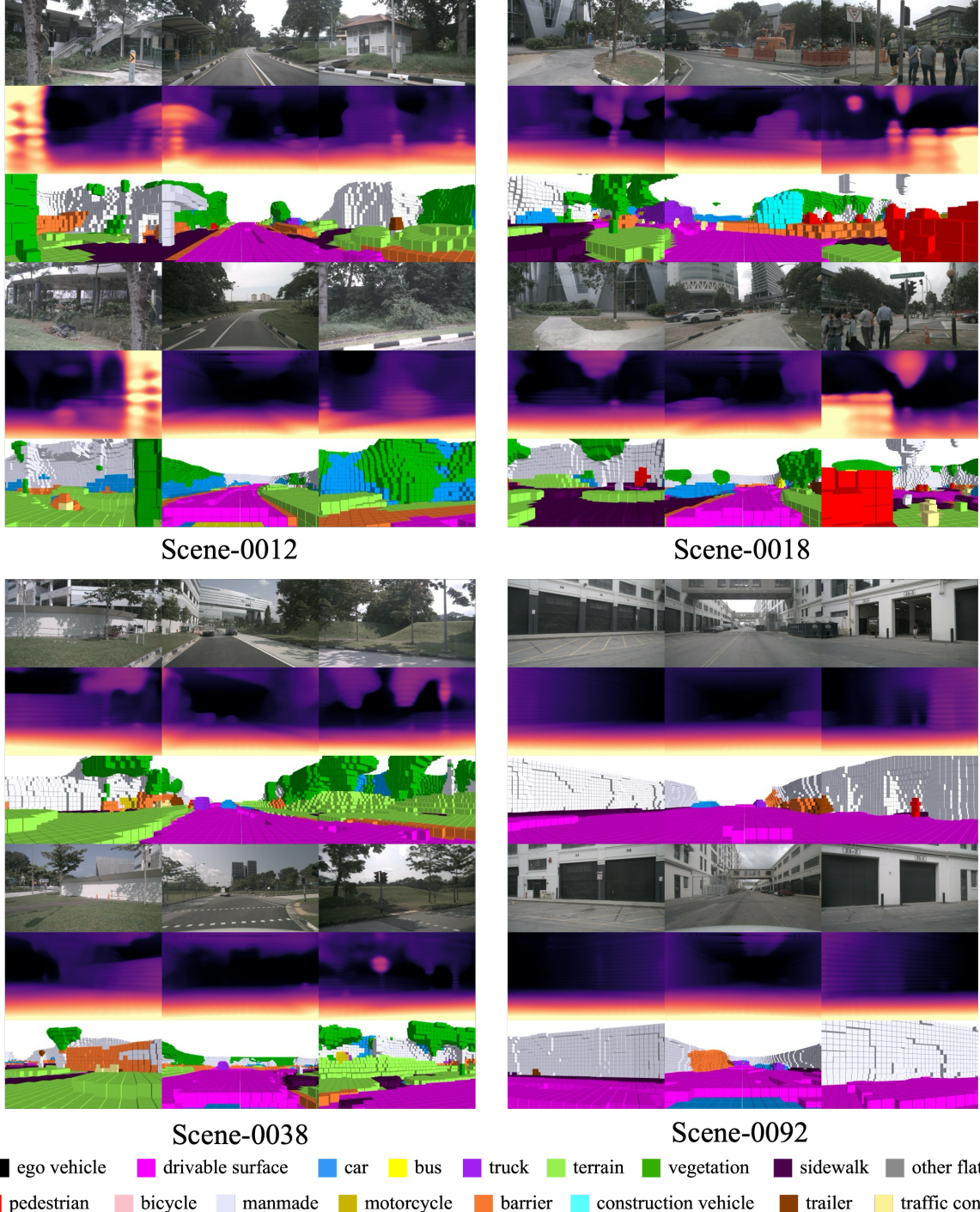


Figure 7. The visualization of the render depth map and 3D occupancy prediction on nuScenes dataset.

- [21] Nan Huang, Xiaobao Wei, Wenzhao Zheng, Pengju An, Ming Lu, Wei Zhan, Masayoshi Tomizuka, Kurt Keutzer, and Shanghang Zhang. S3 gaussian: Self-supervised street gaussians for autonomous driving. *arXiv preprint arXiv:2405.20323*, 2024. 2
- [22] Yuanhui Huang, Wenzhao Zheng, Yunpeng Zhang, Jie Zhou,

and Jiwen Lu. Tri-perspective view for vision-based 3d semantic occupancy prediction. In *CVPR*, pages 9223–9232, 2023. 5, 11

- [23] Yuanhui Huang, Wenzhao Zheng, Borui Zhang, Jie Zhou, and Jiwen Lu. Selfocc: Self-supervised vision-based 3d occupancy prediction. In *Proceedings of the IEEE/CVF Con-*

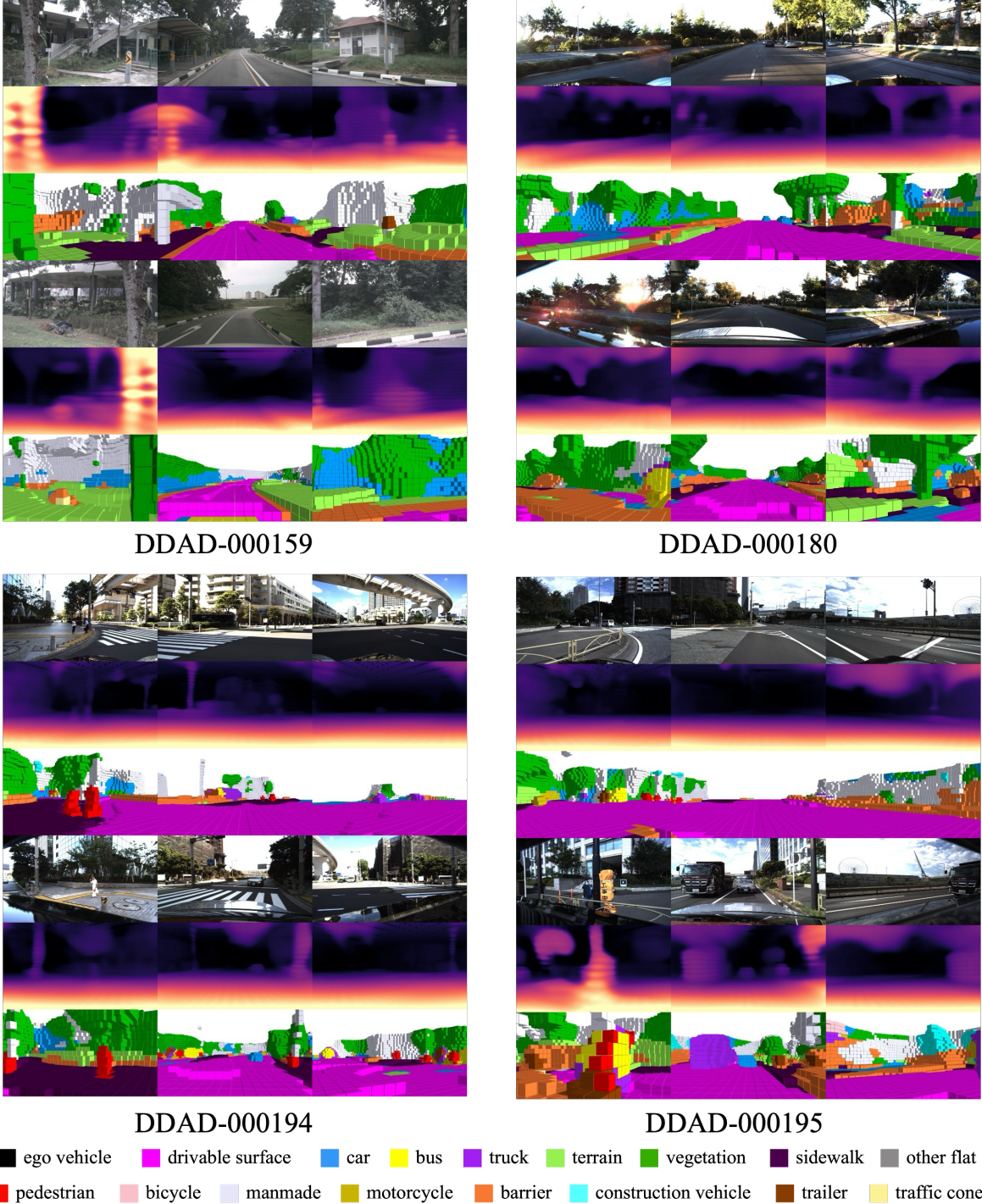


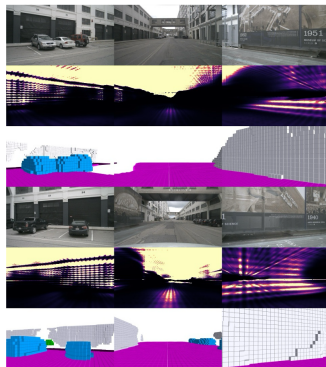
Figure 8. The visualization of the render depth map and 3D occupancy prediction on DDAD dataset

ference on Computer Vision and Pattern Recognition, pages 19946–19956, 2024. 1, 2, 3, 4, 5, 6, 7, 11

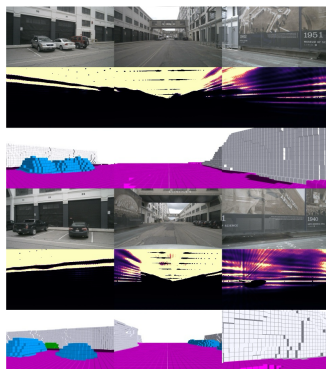
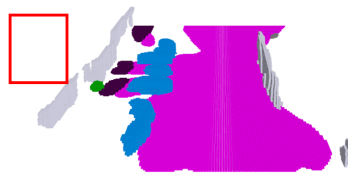
- [24] Yuanhui Huang, Wenzhao Zheng, Yunpeng Zhang, Jie Zhou, and Jiwen Lu. Gaussianformer: Scene as gaussians for vision-based 3d semantic occupancy prediction. *arXiv preprint arXiv:2405.17429*, 2024. 3

[25] Kai Katsumata, Duc Minh Vo, and Hideki Nakayama. An efficient 3d gaussian representation for monocular/multi-view dynamic scenes. *arXiv preprint arXiv:2311.12897*, 2023. 2

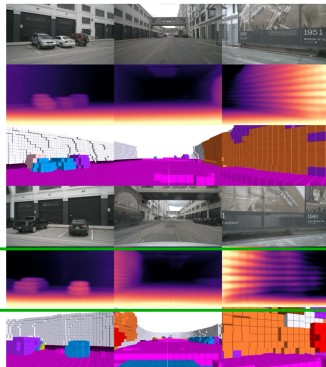
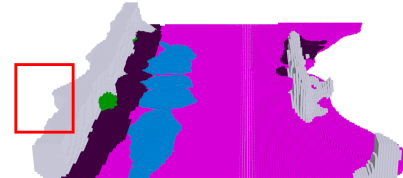
- [26] Bernhard Kerbl, Georgios Kopanas, Thomas Leimkühler, and George Drettakis. 3d gaussian splatting for real-time radiance field rendering. *ACM Trans. Graph.*, 42(4):139–1,



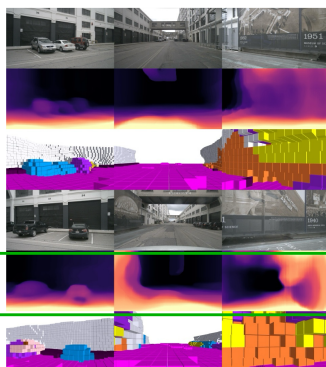
(1) Supervised learning with GT Occ. and without the visible mask



(2) Supervised learning with GT Occ. and with the visible mask



(3) Self-supervised learning with Gaussian splatting rendering (Ours)



(4) Self-supervised learning with Volume rendering (OccNeRF)

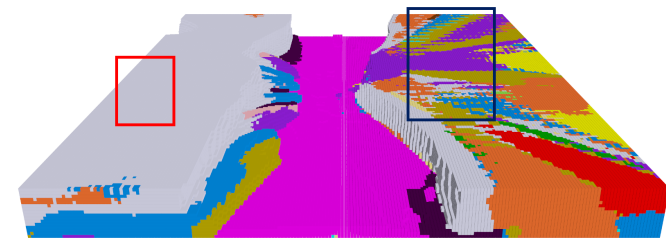


Figure 9. The visualization of the different supervision types (1-4) comparison on nuScenes dataset.

Method	Pretraining setting	mIoU	RayIoU	RayIoU _{1m, 2m, 4m}
Baseline	None	37.29	28.2	22.3 28.7 33.7
Self-supervised pretrain	DDAD nuScenes	37.40 38.45	28.7 29.9	22.9 29.1 34.0 23.9 30.4 35.5

Table 11. The study on SimpleOcc [11] with fully self-supervised pretrain. The baseline is directly training the model with 3D occupancy label. The self-supervised pretraining is conducted on DDAD and nuScenes and then finetuned the model with 3D occupancy label. The number with bold typeface means the best.

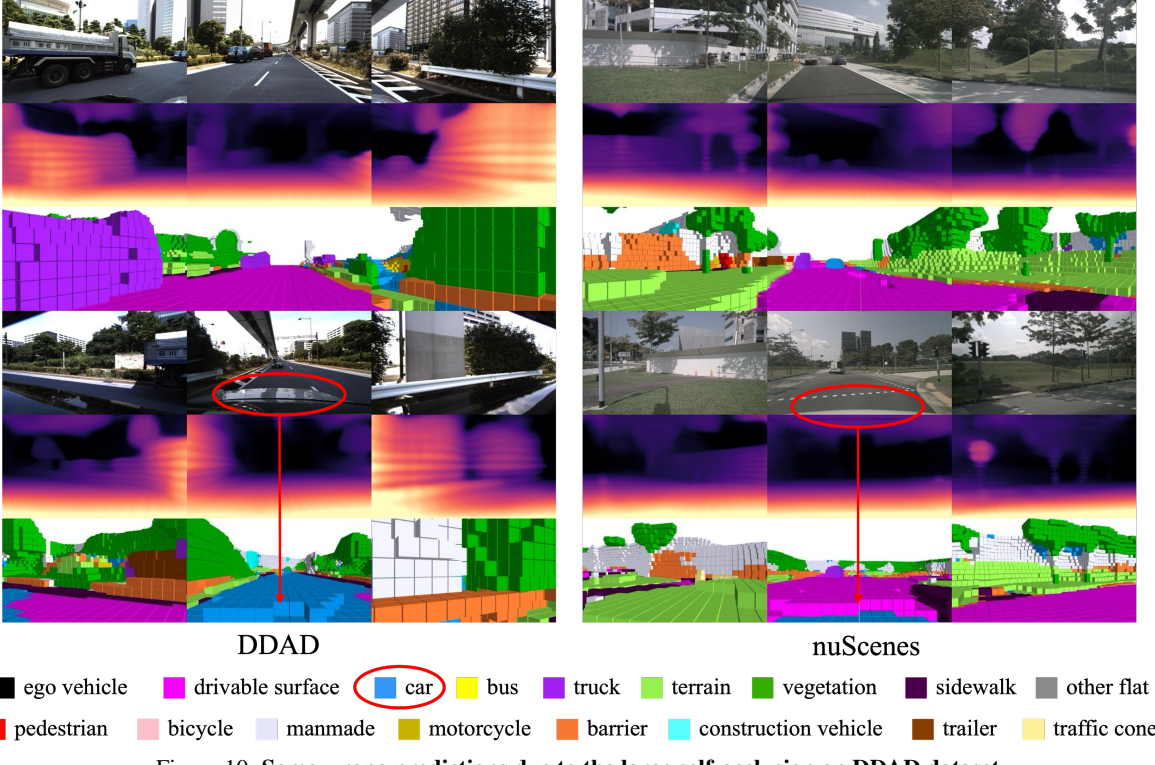


Figure 10. Some wrong predictions due to the large self-occlusion on DDAD dataset.

2023. 2, 3
- [27] Jung-Hee Kim, Junhwa Hur, Tien Phuoc Nguyen, and Seong-Gyun Jeong. Self-supervised surround-view depth estimation with volumetric feature fusion. *NeurIPS*, 35:4032–4045, 2022. 2, 3, 6, 7, 8
- [28] Yinhao Li, Zheng Ge, Guanyi Yu, Jinrong Yang, Zengran Wang, Yukang Shi, Jianjian Sun, and Zeming Li. Bevdepth: Acquisition of reliable depth for multi-view 3d object detection. *arXiv preprint arXiv:2206.10092*, 2022. 1
- [29] Zhiqi Li, Wenhui Wang, Hongyang Li, Enze Xie, Chong-hao Sima, Tong Lu, Qiao Yu, and Jifeng Dai. Bevformer: Learning bird's-eye-view representation from multi-camera images via spatiotemporal transformers. In *ECCV*, 2022. 1, 5, 11
- [30] Zhiqi Li, Zhiding Yu, David Austin, Mingsheng Fang, Shiyi Lan, Jan Kautz, and Jose M Alvarez. Fb-occ: 3d occupancy prediction based on forward-backward view transformation. *arXiv preprint arXiv:2307.01492*, 2023. 2, 11
- [31] Haisong Liu, Haiguang Wang, Yang Chen, Zetong Yang, Jia Zeng, Li Chen, and Limin Wang. Fully sparse 3d panoptic occupancy prediction. *arXiv preprint arXiv:2312.17118*, 2023. 1, 2, 7, 9
- [32] Tianqi Liu, Guangcong Wang, Shoukang Hu, Liao Shen, Xinyi Ye, Yuhang Zang, Zhiguo Cao, Wei Li, and Ziwei Liu. Fast generalizable gaussian splatting reconstruction from multi-view stereo. *arXiv preprint arXiv:2405.12218*, 2024. 2
- [33] Ze Liu, Yutong Lin, Yue Cao, Han Hu, Yixuan Wei, Zheng Zhang, Stephen Lin, and Baining Guo. Swin transformer: Hierarchical vision transformer using shifted windows. In *Proceedings of the IEEE/CVF international conference on computer vision*, pages 10012–10022, 2021. 5
- [34] Yuexin Ma, Tai Wang, Xuyang Bai, Huitong Yang, Yuenan Hou, Yaming Wang, Yu Qiao, Ruigang Yang, Dinesh Manocha, and Xinge Zhu. Vision-centric bev perception: A survey. *arXiv preprint arXiv:2208.02797*, 2022. 1, 2
- [35] Ben Mildenhall, Pratul P Srinivasan, Matthew Tancik, Jonathan T Barron, Ravi Ramamoorthi, and Ren Ng. Nerf:

- Representing scenes as neural radiance fields for view synthesis. In *ECCV*, pages 405–421. Springer, 2020. 1, 2, 4
- [36] nuScenes team. Ego pose discussion. <https://github.com/nutonomy/nuscenes-devkit/issues/961>. Accessed November 12, 2024 [Online], 2023. 7
- [37] Mingjie Pan, Jiaming Liu, Renrui Zhang, Peixiang Huang, Xiaoqi Li, Li Liu, and Shanghang Zhang. Renderocc: Vision-centric 3d occupancy prediction with 2d rendering supervision. *arXiv preprint arXiv:2309.09502*, 2023. 1, 2, 4, 5, 11
- [38] Aron Schmied, Tobias Fischer, Martin Danelljan, Marc Pollefeys, and Fisher Yu. R3d3: Dense 3d reconstruction of dynamic scenes from multiple cameras. In *ICCV*, pages 3216–3226, 2023. 2, 6, 7
- [39] Yining Shi, Kun Jiang, Jiusi Li, Junze Wen, Zelin Qian, Mengmeng Yang, Ke Wang, and Diange Yang. Grid-centric traffic scenario perception for autonomous driving: A comprehensive review. *arXiv preprint arXiv:2303.01212*, 2023. 1, 2
- [40] Stanislaw Szymanowicz, Chrisitian Rupprecht, and Andrea Vedaldi. Splatter image: Ultra-fast single-view 3d reconstruction. In *Proceedings of the IEEE/CVF Conference on Computer Vision and Pattern Recognition*, pages 10208–10217, 2024. 2
- [41] Xiaoyu Tian, Tao Jiang, Longfei Yun, Yue Wang, Yilun Wang, and Hang Zhao. Occ3d: A large-scale 3d occupancy prediction benchmark for autonomous driving. *arXiv preprint arXiv:2304.14365*, 2023. 1, 2, 4, 5, 8, 10, 11
- [42] Wenwen Tong, Chonghao Sima, Tai Wang, Li Chen, Silei Wu, Hanming Deng, Yi Gu, Lewei Lu, Ping Luo, Dahua Lin, et al. Scene as occupancy. In *Proceedings of the IEEE/CVF International Conference on Computer Vision*, pages 8406–8415, 2023.
- [43] Xiaofeng Wang, Zheng Zhu, Wenbo Xu, Yunpeng Zhang, Yi Wei, Xu Chi, Yun Ye, Dalong Du, Jiwen Lu, and Xinggang Wang. Openoccupancy: A large scale benchmark for surrounding semantic occupancy perception. In *ICCV*, 2023. 1, 2
- [44] Yi Wei, Linqing Zhao, Wenzhao Zheng, Zheng Zhu, Yongming Rao, Guan Huang, Jiwen Lu, and Jie Zhou. Surround-depth: Entangling surrounding views for self-supervised multi-camera depth estimation. In *CoRL*, pages 539–549. PMLR, 2023. 2, 3, 5, 6, 7, 9
- [45] Yi Wei, Linqing Zhao, Wenzhao Zheng, Zheng Zhu, Jie Zhou, and Jiwen Lu. Surroundocc: Multi-camera 3d occupancy prediction for autonomous driving. In *ICCV*, pages 21729–21740, 2023. 1, 2
- [46] Felix Wimbauer, Nan Yang, Christian Rupprecht, and Daniel Cremers. Behind the scenes: Density fields for single view reconstruction. In *Proceedings of the IEEE/CVF Conference on Computer Vision and Pattern Recognition*, pages 9076–9086, 2023. 1
- [47] Guanjun Wu, Taoran Yi, Jiemin Fang, Lingxi Xie, Xiaopeng Zhang, Wei Wei, Wenyu Liu, Qi Tian, and Xinggang Wang. 4d gaussian splatting for real-time dynamic scene rendering. In *Proceedings of the IEEE/CVF Conference on Computer Vision and Pattern Recognition*, pages 20310–20320, 2024. 2
- [48] Huaiyuan Xu, Junliang Chen, Shiyu Meng, Yi Wang, and Lap-Pui Chau. A survey on occupancy perception for autonomous driving: The information fusion perspective. *arXiv preprint arXiv:2405.05173*, 2024. 1
- [49] Yunzhi Yan, Haotong Lin, Chenxu Zhou, Weijie Wang, Haiyang Sun, Kun Zhan, Xianpeng Lang, Xiaowei Zhou, and Sida Peng. Street gaussians for modeling dynamic urban scenes. *arXiv preprint arXiv:2401.01339*, 2024. 2
- [50] Yuchen Yang, Xinyi Wang, Dong Li, Lu Tian, Ashish Sirasao, and Xun Yang. Towards scale-aware full surround monodepth with transformers. *arXiv preprint arXiv:2407.10406*, 2024. 6, 7
- [51] Zichen Yu, Changyong Shu, Jiajun Deng, Kangjie Lu, Zongdai Liu, Jiangyong Yu, Dawei Yang, Hui Li, and Yan Chen. Flashocc: Fast and memory-efficient occupancy prediction via channel-to-height plugin. *arXiv preprint arXiv:2311.12058*, 2023. 1, 2
- [52] Weihao Yuan, Xiaodong Gu, Zuozhuo Dai, Siyu Zhu, and Ping Tan. Newcrfs: Neural window fully-connected crfs for monocular depth estimation. In *Proceedings of the IEEE Conference on Computer Vision and Pattern Recognition*, 2022. 4, 5, 6, 7, 8
- [53] Zhenlong Yuan, Jiakai Cao, Zhaoxin Li, Hao Jiang, and Zhaoqi Wang. Sd-mvs: Segmentation-driven deformation multi-view stereo with spherical refinement and em optimization. In *Proceedings of the AAAI Conference on Artificial Intelligence*, pages 6871–6880, 2024. 2
- [54] Chubin Zhang, Juncheng Yan, Yi Wei, Jiaxin Li, Li Liu, Yansong Tang, Yueqi Duan, and Jiwen Lu. Occnerf: Self-supervised multi-camera occupancy prediction with neural radiance fields. *arXiv preprint arXiv:2312.09243*, 2023. 1, 2, 3, 4, 5, 6, 8, 9, 11
- [55] Hao Zhang, Feng Li, Xueyan Zou, Shilong Liu, Chunyuan Li, Jianfeng Gao, Jianwei Yang, and Lei Zhang. A simple framework for open-vocabulary segmentation and detection. *arXiv preprint arXiv:2303.08131*, 2023. 2
- [56] Yunpeng Zhang, Zheng Zhu, and Dalong Du. Occformer: Dual-path transformer for vision-based 3d semantic occupancy prediction. In *ICCV*, 2023. 2, 5, 11
- [57] Shunyuan Zheng, Boyao Zhou, Ruizhi Shao, Boning Liu, Shengping Zhang, Liqiang Nie, and Yebin Liu. Gps-gaussian: Generalizable pixel-wise 3d gaussian splatting for real-time human novel view synthesis. In *Proceedings of the IEEE/CVF Conference on Computer Vision and Pattern Recognition*, pages 19680–19690, 2024. 2, 9
- [58] Xiaoyu Zhou, Zhiwei Lin, Xiaojun Shan, Yongtao Wang, Deqing Sun, and Ming-Hsuan Yang. Drivinggaussian: Composite gaussian splatting for surrounding dynamic autonomous driving scenes. In *Proceedings of the IEEE/CVF Conference on Computer Vision and Pattern Recognition*, pages 21634–21643, 2024. 2